Int. J. Heat Mass Transfer. Vol. 36, No. 8, pp. 2125–2134, 1993
Printed in Great Britain

0017-9310/93 $6.00+0.00

Experimental and numerical analyses of double diffusive natural convection heated and cooled from opposing vertical walls with an initial condition of a vertically linear concentration gradient

KATSUYOSHI KAMAKURA
Toyama National College of Technology, Toyama 939, Japan

and

HIROYUKI OZOE
Institute of Advanced Material Study, Kyushu University, Kasuga 816, Japan

(*Received* 13 *March* 1992 *and in final form* 21 *September* 1992)

Abstract—When a solution having a vertically linear concentration gradient is heated from a vertical wall and cooled from an opposing vertical wall, multi-layered roll cells separated by almost-horizontal sharp interfaces are observed. A Galerkin finite element method was employed for the numerical analyses of this double diffusive convection. Computations were carried out for the Prandtl number $Pr = 6$, the Lewis number $Le = 100$, an aspect ratio $A = 4$, the Rayleigh number $Ra = 10^6$ and a buoyancy ratio $N = 10$ or 20. Multi-layered roll cells with sharp and almost-horizontal interfaces were formed in the numerical simulation and then the concentration in each layer became almost uniform. The experiment confirmed the numerical results.

1. INTRODUCTION

When a solution having a concentration gradient along the gravitational direction is heated from one vertical side wall and cooled from an opposing wall, multi-layered roll cells are formed and small tilted sharp interfaces are observed. This phenomenon has been called double diffusive convection, which occurs in a fluid when density changes are caused by both concentration and temperature gradients.

The study of double diffusive convection was developed by Turner *et al.* [1–3], and most of the earlier experiments were carried out for a stable stratified brine solution heated from below. In these, several layers were formed under certain conditions both near the bottom of the container and further up. Subsequently, different experiments heated from a side wall were also carried out. Then similar multi-layered roll cells were observed and an extensive number of works [4–8] have been reported. Once multi-layered roll cells are formed in the system of lateral heating, they are very stable and separate roll cells exist for long hours because of the slow rate of mass transfer of solute across the interface. Double diffusive phenomenon is important in many fields of engineering. A recent important example is a crystal growth process [9], in which the structure and quality of the solid crystal have been known to be affected profoundly by the liquid convection and the double diffusive convection is induced because of the non-unity distribution coefficient of impurities. Moreover, double diffusive convection has been widely investigated, in various fields such as meteorology, chemistry, astrophysics, geology, etc.

The numerical simulation of double diffusive convection for a single cell was carried out due to Murty [10]. Bergman and Ungan [11] simulated double diffusive motion in a linearly-stratified thermohaline system heated from below in a rectangular box and many cells were observed horizontally. Kamakura and Ozoe [12] reported the simulation of two-layer convection which consists of water and aqueous solution at the beginning. The system was heated and cooled from the opposing side walls stepwise and convection occurred in each layer. A similar simulation to that described in this paper was reported by Heinrich [13, 14]. He simulated the phenomenon in the case of lateral heating in a linearly-stratified thermohaline system in a rectangular box, and multi-layered roll cells were observed. However, his computational work was limited to the formation process of the roll cells. The present work is to clarify the transient formation and degradation processes of roll cells when a solution having an initial linear concentration gradient is heated from one vertical side wall and cooled from an opposing vertical wall. The cal-

NOMENCLATURE

A	aspect ratio, $2H/B$
B	width of a solution in the apparatus [m]
C	dimensionless concentration, $(c-c_0)/\Delta c_{max}$
c	concentration [mol m^{-3}]
c_0	average concentration, $(c_{max}+c_{min})/2$ [mol m^{-3}]
c_{max}	initial maximum concentration [mol m^{-3}]
c_{min}	initial minimum concentration [mol m^{-3}]
D	diffusion coefficient [m^2 s^{-1}]
g	acceleration due to gravity [m s^{-2}]
H	1/2-height of a solution in the apparatus [m]
Le	Lewis number, κ/D
N	buoyancy ratio, $\beta\Delta c_{max}/(\alpha\Delta T_{max})$
Nu_{loc}	local Nusselt number (equation 8)
Nu_{ave}	average Nusselt number (equation 9)
n	dimensionless coordinate normal to the boundary
Pr	Prandtl number, ν/κ
Ra	Rayleigh number, $g\alpha\Delta T_{max}H^3/(\kappa\nu)$
T	temperature [K]
T_{cold}	temperature on the cold wall [K]
T_{hot}	temperature on the hot wall [K]
T_0	average temperature, $(T_{hot}+T_{cold})/2$ [K]
t	time [s]
U	dimensionless velocity, uH/κ
u	velocity in the x-direction [m s^{-1}]
V	dimensionless velocity, vH/κ
v	velocity in the y-direction [m s^{-1}]
X	dimensionless coordinate, x/H
x	horizontal coordinate [m]
Y	dimensionless coordinate, y/H
y	vertical coordinate [m].

Greek symbols

α	volumetric coefficient of thermal expansion [K^{-1}]
β	volumetric coefficient of expansion with concentration [m^3 mol^{-1}]
Δc_{max}	$c_{max}-c_{min}$ [mol m^{-3}]
Δn	dimensionless distance between wall and next node
ΔT_{max}	$T_{hot}-T_{cold}$ [K]
ζ	dimensionless vorticity, $\omega H^2/\kappa$
θ	dimensionless temperature, $(T-T_0)/\Delta T_{max}$
κ	thermal diffusivity [m^2 s^{-1}]
ν	kinematic viscosity [m^2 s^{-1}]
τ	dimensionless time
Ψ	dimensionless stream-function ($U=\partial\Psi/\partial Y$, $V=-\partial\Psi/\partial X$)
ω	vorticity [s^{-1}].

Subscripts

1	one grid space away from the wall
2	two grid spaces away from the wall.

culations are carried out for different buoyancy ratios, and the formation of interfaces is presented in further detail by the fine contours of concentration.

In this paper both numerical and experimental studies are described. Computations were carried out for $Pr = 6$, $Le = 100$, $A = 4$, $Ra = 10^6$ and $N = 10$ or 20. The Prandtl number, the Lewis number and the aspect ratio roughly correspond to the experimental conditions, but the Rayleigh number was arbitrarily chosen for the formation of roll cells. The concentration gradient determines the value of the buoyancy ratio N. The value of $N = 10$ or 20 corresponds to the steep concentration gradient. These buoyancy ratios are the values of the practical systems for which the stable multi-layered convection occurs. The experiment was carried out to compare with the numerical results.

2. MATHEMATICAL MODELS AND BOUNDARY CONDITIONS

The basic equations to describe the double diffusive natural convection consists of the stream-function equation, the vorticity equation, the energy equation and the concentration equation as follows in dimensionless form:

$$\zeta = \frac{\partial V}{\partial X} - \frac{\partial U}{\partial Y} = -\nabla^2\Psi \tag{1}$$

$$\frac{\partial\zeta}{\partial\tau} + U\frac{\partial\zeta}{\partial X} + V\frac{\partial\zeta}{\partial Y} = Ra\,Pr\left(-\frac{\partial\theta}{\partial X} + N\frac{\partial C}{\partial X}\right) + Pr\nabla^2\zeta \tag{2}$$

$$\frac{\partial\theta}{\partial\tau} + U\frac{\partial\theta}{\partial X} + V\frac{\partial\theta}{\partial Y} = \nabla^2\theta \tag{3}$$

$$\frac{\partial C}{\partial\tau} + U\frac{\partial C}{\partial X} + V\frac{\partial C}{\partial Y} = \nabla^2 C/Le. \tag{4}$$

Dimensionless parameters Pr, Ra, Le, N and A are defined as follows:

$$Pr = \frac{\nu}{\kappa}, \quad Ra = \frac{g\alpha\Delta T H^3}{\kappa\nu}, \quad Le = \frac{\kappa}{D}$$

$$N = \frac{\beta\Delta C_{max}}{\alpha\Delta T_{max}}, \quad A = \frac{2H}{B}. \tag{5}$$

Here, the dimensionless variables are defined as

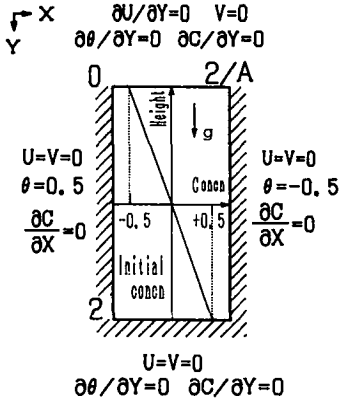

FIG. 1. Boundary conditions.

$$X = x/H, \quad Y = y/H, \quad U = uH/\kappa$$
$$V = vH/\kappa, \quad \tau = t\kappa/H^2, \quad \zeta = \omega H^2/\kappa$$
$$\theta = (T-T_0)/\Delta T_{max}, \quad C = (c-c_0)/\Delta c_{max}. \qquad (6)$$

The following boundary conditions in dimensionless form are illustrated in Fig. 1:

at $Y = 0$:

$$\partial U/\partial Y = 0, \quad V = 0, \quad \partial\theta/\partial Y = 0, \quad \partial C/\partial Y = 0;$$

at $Y = 2$:

$$U = V = 0, \quad \partial\theta/\partial Y = 0, \quad \partial C/\partial Y = 0;$$

at $X = 0$:

$$U = V = 0, \quad \theta = 0.5, \quad \partial C/\partial X = 0;$$

at $X = 2/A$:

$$U = V = 0, \quad \theta = -0.5, \quad \partial C/\partial X = 0.$$

The initial concentration in the system is linearly distributed from $+0.5$ at the bottom to -0.5 at the free top surface.

3. COMPUTATIONAL METHOD

A Galerkin finite element method was used to analyze a transient formation process of multi-layered roll cells with double diffusive natural convection. The rectangular cross-section of the system with a linear concentration gradient is divided into a number of triangles, and the typical mesh of 19×69 nodes is shown in Fig. 2. The mesh is symmetrical. The dimensionless width, 0.5, of the system is divided into 18 portions, and the X-coordinate of the nodes is as follows:

$X = 0,\ 2/164,\ 4/164,\ 7/164,\ 11/164$
$17/164,\ 23/164,\ 29/164,\ 35/164$
$41/164,\ 47/164,\ 53/164,\ 59/164$
$65/164,\ 71/164,\ 75/164,\ 78/164$
$80/164,\ 82/164.$

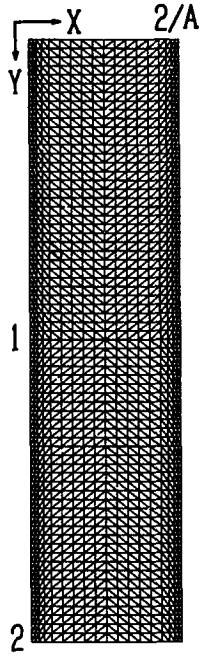

FIG. 2. Finite element mesh with 1311 nodes and 2448 elements.

The dimensionless height, 2, of the system is divided at equal spacings into 48, 58, 68, 78 or 88 portions.

The vorticity on the wall was computed as follows:

$$\zeta = -\frac{\partial^2\Psi}{\partial n^2} = -\frac{3\Psi_1}{\Delta n^2} - \frac{\zeta_1}{2}. \qquad (7)$$

The initial concentration in the system is linearly distributed from $+0.5$ at the bottom to -0.5 at the free top surface.

Computations were carried out for $Pr = 6$, $Le = 100$, $A = 4$, $Ra = 10^6$ and $N = 10$ or 20. The local Nusselt number on the hot wall was calculated from the Taylor series for the temperature field as follows:

$$Nu_{loc} = \frac{(\theta_{hot}-\theta_1)/X_1^2 - (\theta_{hot}-\theta_2)/X_2^2}{1/X_1 - 1/X_2} \cdot \frac{2}{A}. \qquad (8)$$

The average Nusselt number was computed as follows:

$$Nu_{ave} = \frac{1}{2}\int_0^2 Nu_{loc}\, dY. \qquad (9)$$

4. NUMERICAL RESULTS

4.1. *Computational meshes*

The number of nodes may markedly affect the numerical results. When the mesh widths are coarse, the numerical results may be unreliable or vague. As the concentration distribution in the multi-layered convection is almost discontinuous, the computed concentration tends to have irregular values. The solute is transferred vertically and then the concentration

is mainly distributed vertically. Therefore, the division number in the Y-direction is important. To study the effect of mesh width, the computations were carried out for different meshes of 48, 58, 68, 78 and 88 divisions in the Y-direction, as shown in Fig. 3. In the case of $N = 10$, at $\tau = 0.2$ the roll cells were similarly formed for all meshes in order from both surface and bottom to the center. At $\tau = 0.4$ the roll cells are observed in the whole system, but the number of roll cells and the position of interfaces are dependent on the mesh numbers. Nevertheless at $\tau = 0.6$ four roll cells are similarly formed for all cases except for 19×49 nodes.

In the case of $N = 20$, for the meshes of 19×69 and 19×89 nodes two roll cells appeared just below the free surface and just above the bottom respectively, but for the mesh of 19×49 nodes the roll cell near the bottom did not develop. It would be a reasonable compromise to carry out the subsequent computations with 19×69 nodes for the reliable results with minimum number of nodes.

4.2. *Heat transfer*

As shown in Fig. 4, at $\tau = 0.05$ the Nu_{loc} have a variation only near the bottom plane, but at $\tau = 1$ four peaks appear all over the wall from top to bottom to reflect the formation of roll cells.

Figure 5 shows transient response curves of the average Nusselt number, Nu_{ave}. In the case of $N = 10$ which is shown with square symbols, at first the Nu_{ave} increased very greatly with time but later became roughly constant. In the case of $N = 20$ which is shown with black circle symbols, after the induction time the Nu_{ave} increased with time.

4.3. *Computed contours*

Figures 6 and 7 show the instantaneous contours of stream function, temperature and concentration which were obtained by computer simulation. In the case of $N = 10$ (Fig. 6) the formation process of the multi-layered roll cells can be observed and the stable roll cells have almost-horizontal interfaces. In general, at the beginning of the step heating and cooling from the side walls, two roll cells appeared just below the free surface and just above the bottom respectively; the contours of stream function consist of two parts. The roll cells were formed in order from both surface and bottom to the center, and developed to the whole system. At $\tau = 0.6$ all roll cells were unified to four stable roll cells but might finally converge to a single roll cell after a long time with the concentration unification due to diffusion.

In the case of $N = 20$ which is shown in Fig. 7, at first two roll cells appeared just below the free surface and just above the bottom respectively. However, new roll cells were not formed in the mid-height regime. The buoyancy ratio $N = 20$ corresponds to the very steep concentration gradient. Therefore, the two roll cells only developed largely with time below the free surface and above the bottom. The linearly-stratified

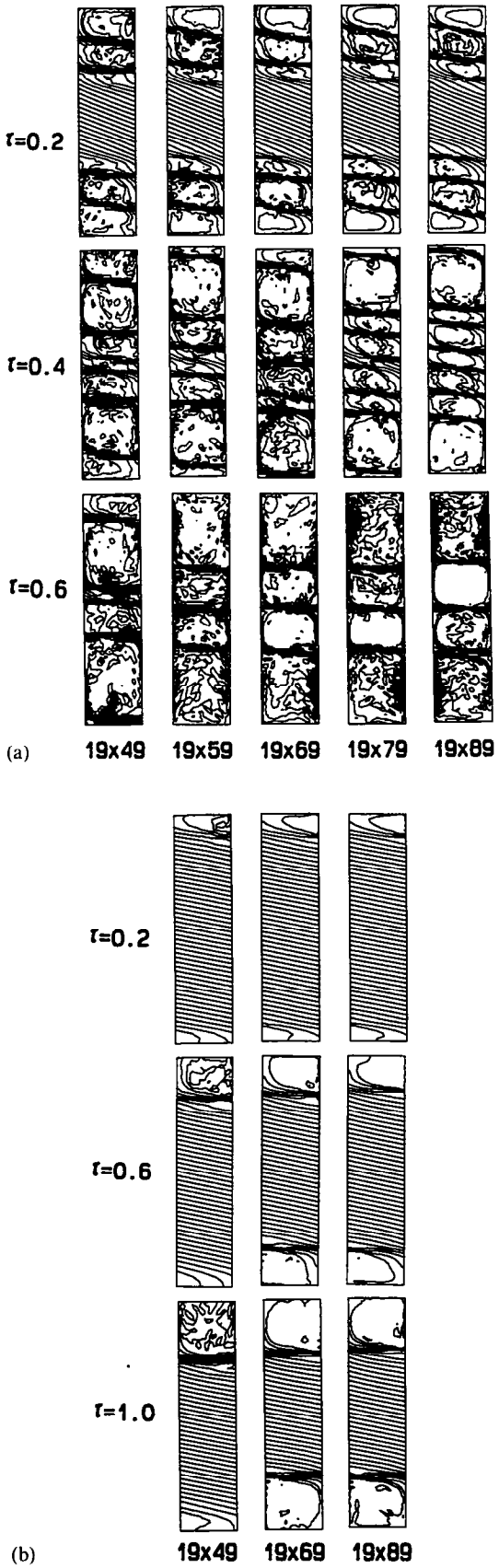

FIG. 3. Instantaneous contours of concentration for different meshes: (a) $Pr = 6$, $Le = 100$, $A = 4$, $Ra = 10^6$ and $N = 10$; (b) $Pr = 6$, $Le = 100$, $A = 4$, $Ra = 10^6$ and $N = 20$.

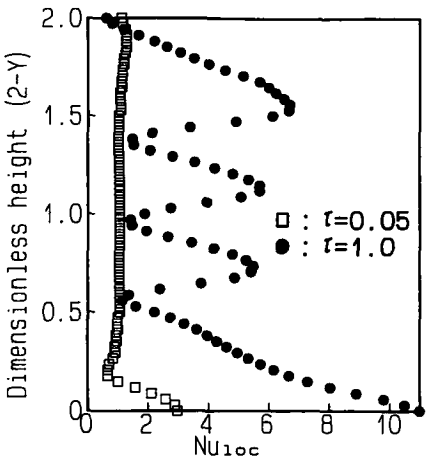

FIG. 4. Instantaneous profiles of the local Nusselt number at $Pr = 6$, $Le = 100$, $A = 4$, $Ra = 10^6$ and $N = 10$.

solution in the mid-height regime might finally disappear and the two-layer system [6, 7, 12] as already reported would be formed.

4.4. *Temperature and concentration profiles*

The vertical profiles of dimensionless temperature and concentration along the vertical center plane at $X = 0.25$ $(= 1/A)$ are plotted at an instance $\tau = 1$ in Fig. 8. The concentration profiles indicated with square symbols are almost uniform in each roll cell. Here are four separate roll cells aligned in a vertical direction. The temperature gradients between roll cells are steep, and the temperature is high at the top in each roll cell and decreases gradually toward the bottom of the cell. Since the convection exists in each layer, the concentration in a layer becomes almost uniform and the concentration gradient is very steep between each cell, as seen in Fig. 8.

4.5. *Mass transfer*

The solute in this system transfers from the lower regime to the upper regime vertically. Once roll cells

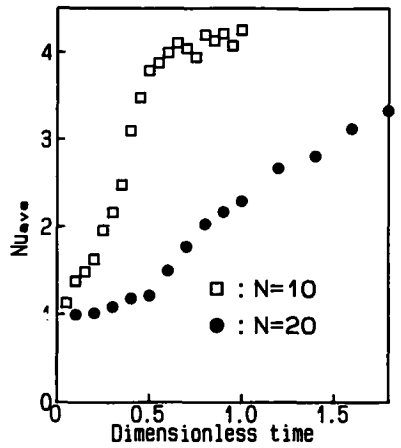

FIG. 5. Transient responses of the average Nusselt number on the hot wall at $Pr = 6$, $Le = 100$, $A = 4$ and $Ra = 10^6$.

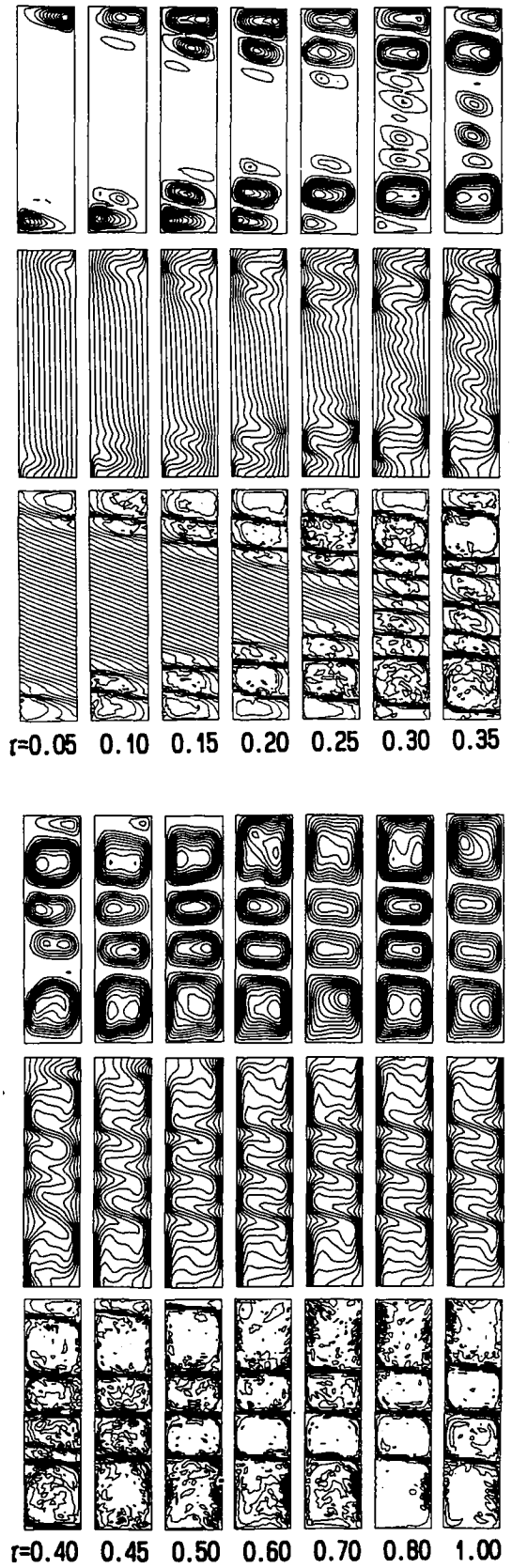

FIG. 6. Transient changes of the instantaneous contours of stream function (top row), temperature (middle row) and concentration (lower row) for $Pr = 6$, $Le = 100$, $A = 4$, $Ra = 10^6$ and $N = 10$.

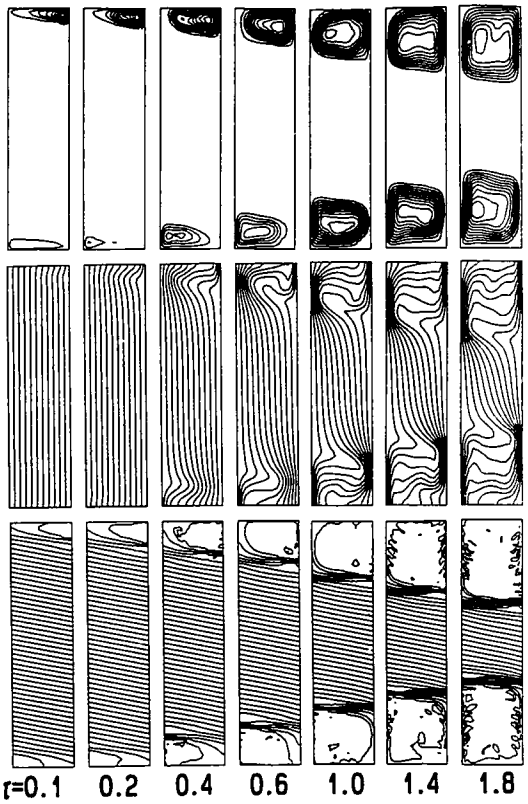

FIG. 7. Transient changes of the instantaneous contours of stream function (top row), temperature (middle row) and concentration (lower row) for $Pr = 6$, $Le = 100$, $A = 4$, $Ra = 10^6$ and $N = 20$.

are established with the large concentration difference between cells, the mass transfer will be carried out through the interfaces both by the diffusion and by the convection. The average concentration in each layer was obtained from the integration of the concentrations in all control volumes. Figure 9 shows the time variation of the average concentration in each layer in the case of $N = 10$. The concentration of the top layer is increasing with time and, on the contrary, that of the bottom layer is decreasing. The circle or triangles in Fig. 9 show the average concentration of roll cells which disappear with time. Please note the concentration is positive in the lower ordinate. However, the concentration of two middle layers are almost constant. Therefore, the concentration difference between the top layer and its lower layer may be decreasing, and similarly the concentration difference between the bottom layer and its upper layer may also be decreasing. The collapse of the roll cells occurs with the disappearance of a roll cell as seen at $\tau = 0.40$–0.60 in Fig. 6. This is because the concentration difference between roll cells becomes small or the thickness of a roll cell becomes small. This phenomenon will be discussed again in the next experimental observation.

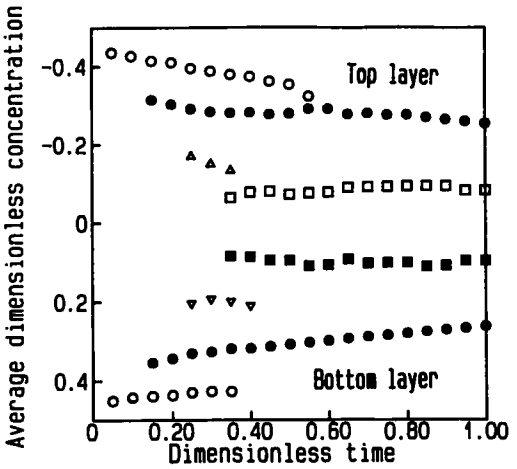

FIG. 9. Time variation of the average concentration in each layer for $Pr = 6$, $Le = 100$, $A = 4$, $Ra = 10^6$ and $N = 10$.

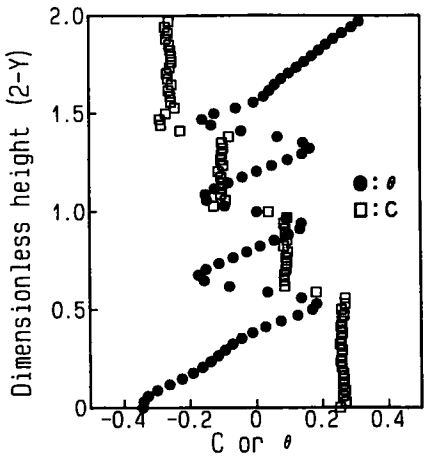

FIG. 8. Vertical profile of dimensionless temperature and concentration at the position of one-half width ($X = 0.5$) for $Pr = 6$, $Le = 100$, $A = 4$, $Ra = 10^6$, $N = 10$ and $\tau = 1.0$.

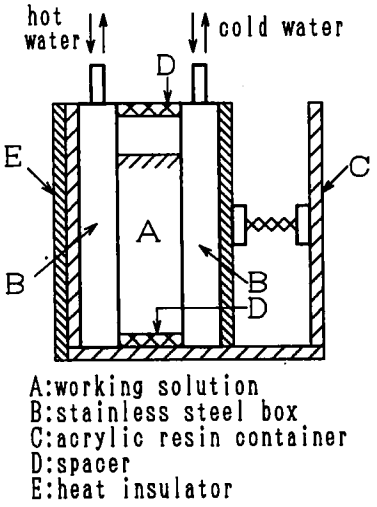

FIG. 10. Experimental apparatus for multi-layered convection.

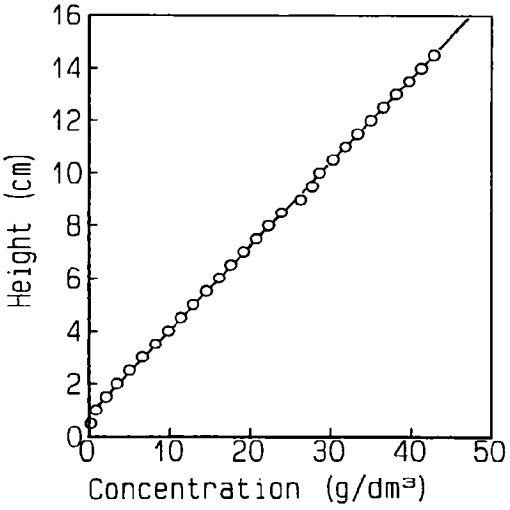

FIG. 11. Concentration profile at the start of heating and cooling.

5. EXPERIMENTAL

5.1. *Materials and apparatus*

The potassium chloride used as a solute is reagent grade and was used without further purification. It was dried at 105°C for 8 h.

Figure 10 shows the apparatus used for measuring multi-layered convection, which is the same as reported already by Kamakura and Ozoe [7]. It consists of two stainless steel boxes ($200 \times 100 \times 40$ mm^3, 0.8 mm thick plate) in which water passes for heating or cooling the wall and of an acrylic resin container for holding the convection media.

5.2. *Procedure*

The water and the solution which were used for the multi-layered convection were degassed by boiling under a reduced pressure. The temperatures of the circulating water used for heating or cooling the wall

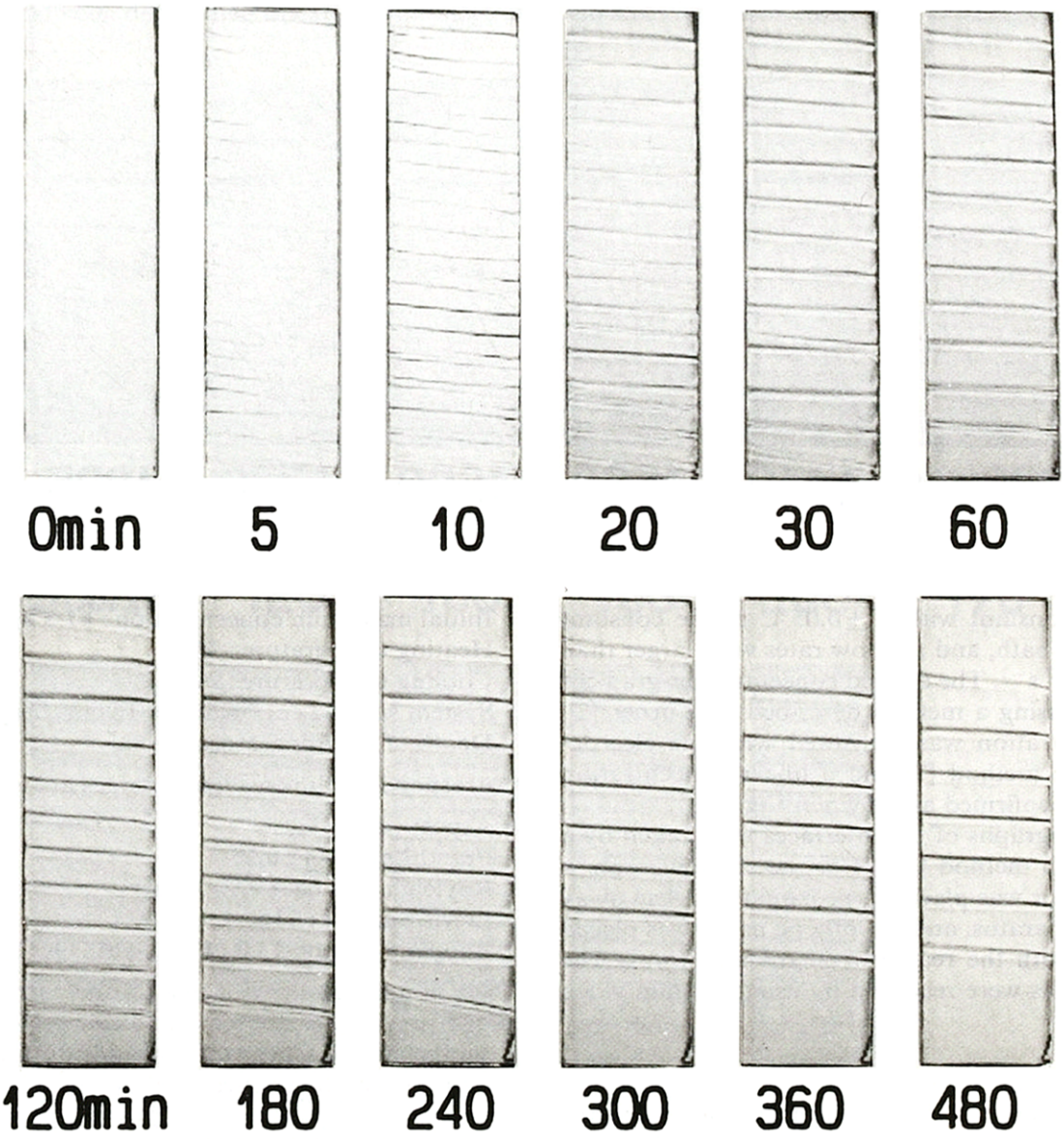

FIG. 12. Shadowgraphs (location of the interfaces). The time is the elapsed time from the start of heating and cooling. (It is also the case in subsequent experiments.) Water—47.5 kg m^{-3} KCl; heating: 30°C, left side; cooling: 20°C, right side; aspect ratio: 4.

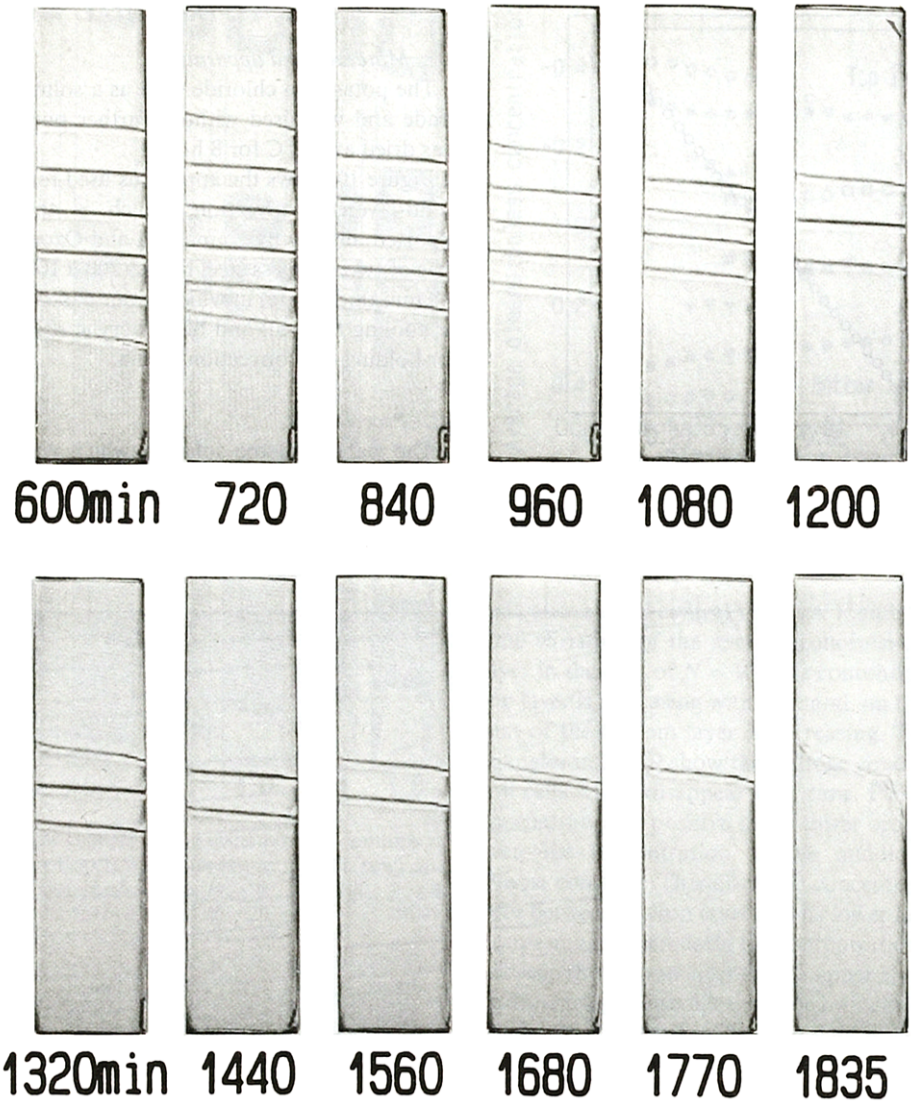

FIG. 12.—*Continued.*

were kept constant within ± 0.05°C in the constant temperature bath, and the flow rates were larger than 1.5×10^{-4} m^3 s^{-1}. The desired concentration-gradient was set up using a method described by Turner [2]. The concentration was measured with the electric-conductance method [7] and a linear concentration profile was confirmed as shown in Fig. 11.

The photographs of the interfaces were taken by a shadowgraph method [15]. For the shadowgraph, a slide projector was placed approximately 2.1 m away from the apparatus, and a synthetic paper was placed in contact with the rear wall of the apparatus. The shadowgraphs were recorded by using a 8 mm video camera.

5.3. *Experimental conditions*

The experiment of double diffusive convection for the system with a linear concentration gradient was carried out for the following conditions:

Initial minimum concentration: water;
Initial maximum concentration: 47.5 kg m^{-3} KCl;
Heating temperature: 30°C;
Cooling temperature: 20°C;
System sizes: 4 cm (width) × 16 cm (height);
Depth of the apparatus: 10 cm.

Corresponding dimensionless values are as follows:

Aspect ratio: 4;
Prandtl number: 6.27;
Rayleigh number: 9.23×10^7;
Lewis number: 71.8;
Buoyancy ratio: 13.0 (47.5 kg m^{-3} KCl).

These conditions are not one-to-one correspondence to the previous numerical conditions. However, the general characteristics of this double diffusive natural convection can be verified as shown herein.

6. EXPERIMENTAL RESULTS

The multi-layered convection was carried out for the system of linear concentration-gradient from 0 kg

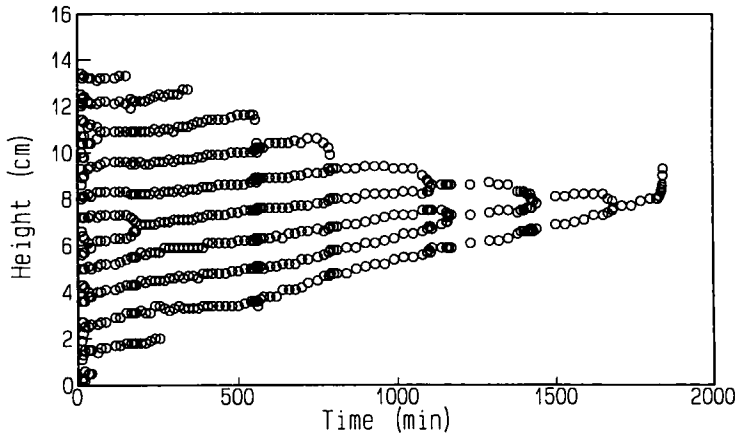

FIG. 13. Transient location of the interfaces between roll cells. Conditions: same as in Fig. 12.

m^{-3} at the top free surface to the 47.5 kg m^{-3} KCl at the bottom. Figure 12 is the shadowgraphs of roll cells in multi-layered convection. The concentration in the apparatus had been distributed linearly at the start of convection (Fig. 11 or 0 min in Fig. 12). Five minutes after the heating and the cooling of the side walls many interfaces appeared in the whole system and the thicknesses of each layer was very shallow. The

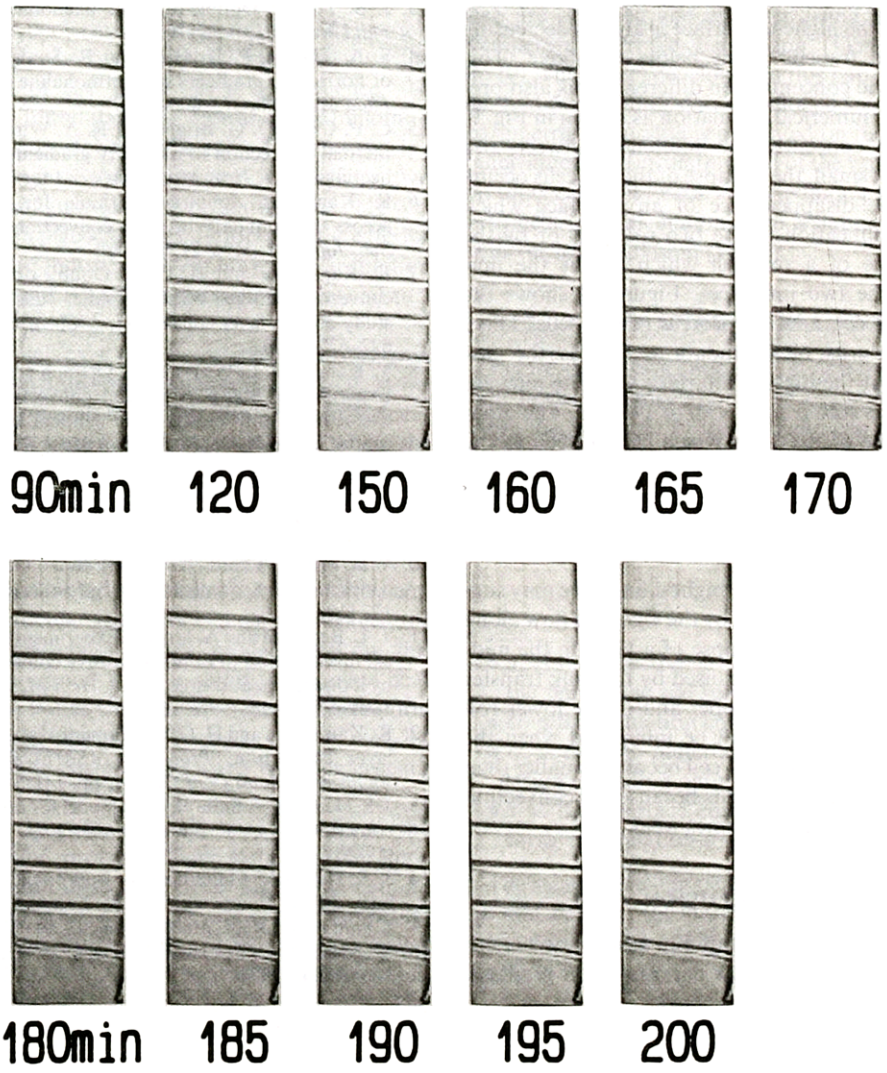

FIG. 14. Shadowgraphs (detailed degradation of the interfaces). Conditions: same as in Fig. 12.

interfaces are relatively largely inclined. The number of interfaces decreased with time and the thicknesses of each roll cell gradually increased. About 60 min later the thicknesses became approximately constant. In the subsequent convection the thickness of the roll cells was kept approximately constant except for both the top and the bottom layers. This fact appears to support the previous numerical results as seen at $\tau \geqslant 0.5$ in Fig. 6. The number of interfaces decreased gradually with the degradation of roll cells. The multi-layered convection roll cells finally converged to a single roll convection about 30 h later as seen in Fig. 12.

The locations of interfaces were measured from a series of pictures and summarized in Fig. 13. As seen from these plots, the thickness of each layer was kept almost constant except for both the top and the bottom layers. However, the locations of interfaces moved upward gradually with the lapse of time. Except for the initial degradation, most degradations of roll cells happened at the highest interface except the top surface. These facts can be considered to be related to mass transfer, because the concentration difference at the highest interface is always decreasing by the mass transfer from below to above. This decrease in the concentration difference was also predicted in the numerical simulation as shown in Fig. 9.

When the concentration difference between roll cells becomes small, the collapse of the roll cells occurs either by the disappearance of an interface which means the unification of the two roll cells or by the disappearance of a roll cell which means the unification of the two interfaces. Figure 14 shows the details of the degradation process of roll cells. There are two patterns of degradation. One is the disappearance of the highest interface with the increase of the slope as seen from $t = 90$ to 170 min. The other is the collapse of the layer which can be seen at the middle height from 190 to 200 min. Two interfaces unify with the disappearance of a roll cell. The latter case is also seen in the numerical results at $\tau = 0.35$–0.45 in Fig. 6.

The disappearance of the highest interface may suggest the penetration of fluid by the vigorous flow along the vertical walls. The collapse of a layer in the mid-height regime seems to be caused by the bulk transfer from one roll cell to the upper and/or the lower roll cells. The bulk transfer will be intensified when the thickness of any specific roll cell becomes smaller than those of the adjacent roll cells because the convection of any specific roll cell becomes weak.

7. CONCLUSION

A finite element computational study was carried out for the system of linear concentration-gradient. At first two cells appeared below the free surface and above the bottom respectively. In the case of $N = 10$ several roll cells were formed between the two layers in order from both surface and bottom, and developed to the whole system. However, in the case of $N = 20$ new roll cells were not formed in the mid-height regime, but the two roll cells developed largely with time below the free surface and above the bottom. Experiments were carried out for KCl water solution. Multi-roll cells appeared only 5 min after the heating and degraded to a single roll after 30 h. The process of formation and degradation obtained from the experiment assured the numerical simulation at least approximately.

REFERENCES

1. J. S. Turner and H. Stommel, A new case of convection in the presence of combined vertical salinity and temperature gradients, *Proc. U.S. Nat. Acad. Sci.* **52,** 49–53 (1964).
2. J. S. Turner, The behaviour of a stable salinity gradient heated from below, *J. Fluid Mech.* **33,** 183–200 (1968).
3. J. S. Turner, Double-diffusive phenomena, *Ann. Rev. Fluid Mech.* **6,** 37–56 (1974).
4. S. A. Thorpe, P. K. Hutt and R. Soulsby, The effect of horizontal gradients on thermohaline convection, *J. Fluid Mech.* **38,** 375–400 (1969).
5. C. F. Chen, D. G. Briggs and R. A. Wirtz, Stability of thermal convection in a salinity gradient due to lateral heating, *Int. J. Heat Mass Transfer* **14,** 57–65 (1971).
6. K. Kamakura, Empirical formula for mass transfer across the boundary between convections, *Bull. Chem. Soc. Japan* **52,** 2175–2177 (1979).
7. K. Kamakura and H. Ozoe, Double-diffusive natural convection between vertical parallel walls: experimental study on two-layer convection, *J. Chem. Eng. Japan* **24,** 622–627 (1991).
8. Y. Kamotani, L. W. Wang, S. Ostrach and H. D. Jiang, Experimental study of natural convection in shallow enclosures with horizontal temperature and concentration gradients, *Int. J. Heat Mass Transfer* **28,** 165–173 (1985).
9. S. Ostrach, Fluid mechanics in crystal growth—the 1982 Freeman Scholar lecture, *J. Fluids Engng* **105,** 5–20 (1983).
10. V. D. Murty, A finite element solution of double diffusive convection, *Int. Commun. Heat Mass Transfer* **15,** 165–177 (1988).
11. T. L. Bergman and A. Ungan, Experimental and numerical investigation of double-diffusive convection induced by a discrete heat source, *Int. J. Heat Mass Transfer* **29,** 1695–1709 (1986).
12. K. Kamakura and H. Ozoe, Numerical analyses for two-layer convection, *Proc. 3rd ASME/JSME Thermal Engineering Joint Conf.*, Vol. 1, pp. 141–146 (1991).
13. J. S. Heinrich, A finite element model for double diffusive convection, *Int. J. Numer. Meth. Engng* **20,** 447–464 (1984).
14. J. S. Heinrich, Finite element approximation to buoyancy-driven flows with cyclic boundary conditions, *Comp. Meth. Appl. Mech. Engng* **48,** 91–100 (1985).
15. W. Merzkirch, *Flow Visualization*, p. 76. Academic Press, New York (1974).